1 Title page

Effect of colloidal particle size on physicochemical properties and aggregation behaviors of two alkaline soils

Yu-yang Yan[1], Xin-ran Zhang[1], Chen-yang Xu[1,2]*, Jun-jun Liu[1], Fei-nan Hu[3,4], Zeng-chao Geng[1,2]

(1. *College of Natural Resources and Environment, Northwest A&F University, Yangling, Shaanxi 712100, China*; 2. *Key Laboratory of Plant Nutrition and the Agri-environment in Northwest China, Ministry of Agriculture, Northwest A&F University, Yangling, Shaanxi 712100, China; 3. State Key Laboratory of Soil Erosion and Dryland Farming on the Loess Plateau, Northwest A&F University, Yangling, Shaanxi 712100, China; 4. Institute of Soil and Water Conservation, Chinese Academy of Sciences, Ministry of Water Resources, Yangling, Shaanxi 712100, China*)

*Corresponding author:

Chen-yang Xu

Email address: xuchenyang@nwafu.edu.cn, xuchenyang.ms@163.com;

Postal address: College of Natural Resources and Environment, Northwest A&F University, No. 3 Taicheng Road, Yangling District, Shaanxi 712100, China.

Abstract

Colloidal particles are the most active soil components, and they vary in elemental composition and environmental behaviors with the particle size due to the heterogenous nature of natural soils. The purposes of the present study are to clarify how particle size affects the physiochemical properties and aggregation kinetics of soil colloids, and to further reveal the underlying mechanisms. Soil colloidal fractions, from two alkaline soils—Anthrosol and Calcisol were subdivided into three ranges: $d < 2$ μm, $d < 1$ μm and $d < 100$ nm. The organic and inorganic carbon contents, clay mineralogy, surface electrochemical properties, including surface functional groups and zeta potentials, were characterized. Through time-resolved light scattering technique, the aggregation kinetics of soil colloidal fractions were investigated, and their critical coagulation concentrations (CCCs) were determined. With decreasing colloidal particle diameter, the total carbon content, organic carbon, organic functional groups content and illite content all increased. The zeta potential became less negative and the charge variability decreased with decreasing particle diameter. The CCC values of Anthrosol and Calcisol colloids followed the descending order of $d < 100$ nm, $d < 1$ μm, $d < 2$ μm. Compared with the course factions ($d < 1$ μm and $d < 2$ μm), soil nanoparticles were more abundant in organic carbon and more stable clay minerals ($d < 100$ nm), thus they exhibited strongest colloidal suspension stability. The differences in organic matter contents and clay mineralogy are the fundamental reasons for the differences in colloidal suspension stability behind the size effects of Anthrosol and Calcisol colloids. The present study revealed the size effects of two alkaline soil colloids on carbon content, clay minerals,

42 surface properties and suspension stability, emphasizing that soil nanoparticles are

43 prone to be more stably dispersed instead of being aggregated. These findings can

44 provide references for in-depth understanding of the environmental behaviors of the

45 heterogeneous soil organic-mineral complexes.

46 **Keywords:** Nanoparticles; Clay mineral composition; zeta potential; Critical

47 coagulation concentration

1. Introduction

Soils contain a series of solid particles in continuous sizes, ranging over six orders of magnitude from nanometers to millimeters (Lead and Wilkinson, 2006; Li et al., 2011), among which soil colloids are the most reactive fractions. Soil colloids are characterized by high surface area and abundant surface charges, exhibiting high potential for carbon sequestration and strong adsorption capacity, which can largely determine the fate and transport of pathogens, nutrients, heavy metals and organic pollutants, and might cause environmental problems to adjacent water bodies or groundwater (Baalousha et al., 2009; Calabi-Floody et al., 2011). Due to their high reactivity and fluidity in aqueous environment, soil colloids play an important role in physical, chemical and biogeochemical processes in natural environment (Schäfer et al., 2012; Mayordomo et al., 2016). The capacity of soil colloids in mobilizing bound nutrients and pollutants is closely related to their dispersion stability under various environmental conditions (Won and Burns, 2018). Therefore, studies on the dispersion stability of soil colloids have attracted extensive attention.

Currently, the definition of soil and environmental colloidal fractions is ambiguous. Soil colloidal fractions are defined as soil particles in diameter of < 1 μm (Lead and Wilkinson, 2006; Weil and Brady, 2016), and also being of < 2 μm (Zhang et al., 2021); while in some extreme cases, they can refer to the particles in diameter of 5–10 μm (Yin et al., 2010). Such discrepancies are seen among publications due to the fact that colloids are defined based on the particle diameter range within which they can display colloidal properties. Since for different materials, e.g., metal (Fe/Al/Ti) oxides, silica

70   gel, phyllosilicates, the specific colloidal range differs greatly.

71   Compared with engineered nanoparticles with known mineralogical organization,

72   natural soils are much more heterogeneous (Cárdenas et al., 2010); their elemental

73   composition and clay mineralogy of soil colloids change with particle size. Tsao et al.,

74   (2013) found that quartz and feldspar were mainly dominant in colloidal particles of <

75   2 μm and 450–2000 nm in red soil (Ferralsols, WRB, IUSS Working Group WRB.

76   2022), while illite and montmorillonite were the main clay minerals in nanoparticles

77   (1–100 nm). In addition, the mineral structure at nanometer scale also changes.

78   Compared with colloidal particles of < 2 μm, the Si/Al ratio in nanoparticles increased,

79   and the surface area, morphology, crystallinity, surface atomic structure and frame

80   structure were significantly different (Tsao et al., 2011). Furthermore, particle size also

81   affects the surface potential of soil colloids. Tang et al., (2015) investigated the surface

82   potential variations with particle size (1–10 μm, 0.5–1 μm, 0.2–0.5 μm, < 0.2 μm) for

83   variably-charged yellow soil (Lixisols) and permanently-charged purple soil

84   (Leptosols); among the colloidal fractions, the absolute surface potential of the finest

85   particles of purple soil (Leptosols) was lowest while that of the yellow soil (Lixisols)

86   was the largest, caused by the differences in surface charge density. Thus, the influences

87   of particle size on elemental composition and surface properties of soils should be

88   further studied.

89   In recent years, great progress has been made in the study of dispersion stability

90   of soil clay minerals, such as montmorillonite, kaolinite, illite or hematite, and soil

91   nanoparticles (Xu et al., 2018; Sun et al., 2020; Wei et al., 2021; Zhu et al., 2014). He

92　et al., (2008) demonstrated that hematite nanoparticles with various particle diameters

93　showed different surface properties and aggregation behaviors under the same pH

94　conditions; moreover, the critical coagulation concentrations (CCCs) of hematite

95　decreased with the decrease of particle diameter. Zhou et al., (2013) compared the

96　CCCs of ten different TiO_2 nanoparticles with varying sizes and indicated that crystal

97　structure and particle diameter both affected the aggregation behaviors of TiO_2. Zhang

98　et al. (2016) confirmed that the types of clay minerals for two Alfisols changed from

99　smectite and vermiculite to kaolinite and illite when the particle size varied from

100　colloids to nanoparticles. Therefore, the dependence of physiochemical properties,

101　surface properties and environmental behaviors on particle size for heterogeneous soil

102　colloidal particles needs systematic investigation.

103　　In the present study, soil colloidal particles of two alkaline soils—Anthrosol sand

104　Calcisols were subdivided into three ranges: $d < 2$ μm, $d < 1$ μm and $d < 100$ nm. Their

105　organic fraction and clay mineralogy, surface electrochemical properties and colloidal

106　stability were studied. This study selected two representative calcareous soils to verify

107　the following scientific hypothesis: soil colloids are organic-inorganic composites. As

108　particle diameter decreases (from colloid particles to nanoparticles), the number of

109　organic functional groups on the surface of soil colloids increases, and the type of clay

110　minerals shifts towards finer clay particles, e.g. illite, resulting in increased specific

111　surface area and decreased charge density, and thus enhanced suspension stability,

112　meaning particle diameter influences the composition of soil colloidal fractions,

113　thereby changing surface properties and suspension stability. The findings can have

important implications for predicting the environmental performances of colloids and colloid-facilitated nutrients, pollutes and pathogens in natural soil and water environment.

2. Materials and methods

2.1 Soil sampling

The study collected two surface soil samples (0–20 cm), Lou soil and Cinnamon soil, being the most common and characteristic calcareous soils, by mixing soils form 5–10 sampling points using a stainless-steel auger at Yangling District (N38°18′14″ and E108°2′30″), and Zhouzhi Country (N34°8′8″ and E108°3′10″), on the Guanzhong Plain, in Shaanxi province, northwest China, respectively. Among these, Lou soil, as a unique calcareous soil, have formed on the basis of cinnamon soil through long-term anthropogenic maturation. According to World Reference Base for Soil Resources (WRB, IUSS Working Group WRB. 2022), the Lou soil and Cinnamon soil are classified as Calcic Protocalcic Calcisols (Loamic, Lixic, Humic) and Hortic Endoanthric Anthrosols (Loamic, Luvic, Eutric, Calcic), respectively. Both types of soil developed from loess parent material. The typical soil profile configuration for the tested Anthrosols is Ap1-Ap2-Bt-Bk-C, while for the Calcisols, it is Ah-Bt-Bk-C.

Soils samples were taken back to the laboratory for air-drying and sieving. The basic soil properties were determined based on standard methods. Soil pH was measured with a pH electrode, employing a solution-to-soil ratio of 2.5:1. Soil organic carbon (SOC) was determined using the $K_2Cr_2O_7$ oxidation method. The cation exchange capacity (CEC) of soil was measured with exchange method. The $CaCO_3$

content was determined by gasometric method. The free Fe/Al oxides were extracted by dithionite-citrate-bicarbonate (DCB) solution. The particle size distribution was measured using the laser diffractometer of Malvern Mastersizer 2000 (Malvern Instruments Ltd., UK). The pH of Anthrosols was 8.34 while it was 8.32 for Calcisols. The SOC of Anthrosols and Calcisols were 7.25 $g·kg^{-1}$ and 9.22 $g·kg^{-1}$, respectively. The CEC of Anthrosols and Calcisols were 25.9 $cmol·kg^{-1}$ and 22.2 $cmol·kg^{-1}$.The contents of $CaCO_3$ in Anthrosols and Calcisols were 51.7 $g·kg^{-1}$ and 82.5 $g·kg^{-1}$. The Free Fe/Al oxides content of Anthrosols and Calcisols were 22.8 $g·kg^{-1}$ and 23.1 $g·kg^{-1}$. The proportions of Sand (2–0.02 mm), Silt (0.02–0.002 mm) and Clay (<0.002 mm) in Anthrosols were 34.0%, 40.6% and 25.4% while those were 28.0%, 44.8% and 27.2% for the Calcisols.

2.2 Extraction of soil colloidal fractions in different size ranges

The soil colloidal particles were extracted based on the Stokes' law, and detailed procedures can be found in our previous publication (Hu et al., 2022). Briefly, 50 g of dry soil was weighed into a beaker containing 500 mL of distilled water, and put the suspension under sonication for an hour using the ultrasonic cell disrupter (XO-900D, Nanjing Xianou Instruments Corporation, China) while maintaining the temperature below 30°C. Afterwards, the suspension was transferred to a larger beaker and distilled water was added to make up the total volume of 5 L. The suspension was further dispersed using an electronic blade stirrer (JB-200, Shanghai Nanhui Huiming Apparatus, China) for one hour, before being sieved through sieve with a pore size of 53 μm, and the upper suspensions containing soil colloidal particles in different

158   diameters were collected by centrifugation. Based on the equation (1), centrifugation

159   speed and time for colloidal particles of $d < 2$ μm, < 1 μm and < 100 nm were calculated

160   and shown in Table S1.

161
$$t = \frac{\eta \lg \frac{R_2}{R_1}}{3.81 N^2 r^2 \Delta d}$$
(1)

162   in which, t is time for centrifugation (s); R_1 is the distance from the surface of the liquid

163   to the center of the axis of the centrifuge, here is 5.7 cm; R_2 is distance from the particles

164   to the center of the axis of the centrifuge, here is 10.5 cm; N (rev·s^{-1}) is the centrifuge

165   speed; r (cm) is the desired colloidal particle radius; Δd is the difference in density

166   between the soil particles (2.65 g·cm^{-3}) and water (1 g·cm^{-3}), while Δd is 1.65 g·cm^{-3};

167   η is the water viscosity coefficient, here is 0.00839 g·cm^{-1}·s^{-1} at 25 °C.

168   **2.3 Characterization of soil colloidal fractions in different size ranges**

169   The initial particle diameters of soil colloids were determined by a time-resolved

170   dynamic light scattering (DLS) apparatus (Nanobrook Omni, Brookhaven, USA), each

171   sample was measured 15 times to get the initial particle diameters. The organic carbon

172   contents in soil colloids were determined by potassium dichromate external heating

173   method and total carbon content was determined by elemental analyzer (Elementar

174   Vario EL III, Germany). Total carbon and organic carbon are the averaged results of 3

175   measurements each. The inorganic carbon content was calculated by subtraction

176   method (Wang et al., 2011). The clay mineralogy of soil colloids was determined by the

177   XRD (Ultima-IV, Rigaku, Japan), and by comparing the intensity of the dominant X-

178   ray diffraction peak of the soil mineral colloid to a standard mineral reference (Database

179   ICDD 2004), the relative percentage content of the minerals was determined. The

180   specific surface areas of the soil colloids were measured by BET-N_2 method (ASAP

181   2460, Micromeritics instrument, USA). High-resolution spectra of C1s and O1s of soil

182   colloids were acquired by X-ray photoelectron spectroscopy (XPS) (Thermo Scientific

183   K-Alpha, USA) (Luo et al., 2019), and the Gaussian−Lorentzian curve-fitting program

184   (XPSPEAK 4.1) was used to analyze the XPS spectra. The zeta potentials of soil

185   colloids were measured by Zeta PALS equipped with a BI-ZTU Autotitrator (ZetaPALS,

186   Brookhaven, USA) with 1 mmol·L^{-1} NaCl solution as the background electrolyte, and

187   the pH range of colloidal suspension was set to 3–10 adjusted with 0.1 mol·L^{-1} HCl

188   and NaOH. Each sample was measured six times to get the average zeta potential values.

189   The concentrations of K^+, Na^+, Ca^{2+}, and Mg^{2+} in soil colloidal suspensions were

190   measured by flame atomic absorption spectrophotometry (PinAAciie 900F, USA).

191   **2.4 Aggregation kinetics of soil colloidal fractions**

192   The aggregation kinetic curves of soil colloidal particles in different electrolytes

193   were determined by time-resolved DLS measurements. The incident wavelength was

194   635 nm and the scattering angle was 90°. The stock colloidal suspensions with particle

195   concentration of 200 mg·L^{-1} were mixed with electrolyte solutions with equal volume.

196   The suspension pH was adjusted to 8.0, which was close to the pH value of natural soil

197   with addition of 0.1 mol·L^{-1} HCl or NaOH before measurement. The chosen electrolyte

198   concentrations for NaCl and $CaCl_2$ were 200–2000 and 2–20 mmol·L^{-1}. The effective

199   diameter (D_h) of the mixed sample was automatically recorded every 2 min, and an

200   aggregation kinetic curve was obtained in 30 min monitoring. According to generally

2.5 Calculation of critical coagulation concentration

According to the particle interaction theory, the aggregation kinetic curves under

electrolyte conditions can be divided into reaction-limited aggregation (RLA) stage

under low concentration which was affected by electrolyte conditions and diffusion-

limited aggregation (DLA) stage under high concentration which was not affected by

electrolyte concentration. The CCC is the critical electrolyte concentration when the

aggregation process changes from the RLA state ($\alpha < 1$) to the DLA state ($\alpha = 1$).

Attachment efficiency (α) represents the bonding probability of particle collisions and

can be calculated for each electrolyte concentration by using equation 2, which allowed

the curve of α as a function of electrolyte concentration to be plotted (Xu et al., 2020a;

Hu et al., 2022).

$$\alpha_{\exp} = \frac{1}{W} = \frac{k_{11}}{\left(k_{11}\right)_{fast}} = \frac{\frac{1}{N_0}\left(\frac{\mathrm{d}a_h(t)}{\mathrm{d}t}\right)_{t\to 0}}{\frac{1}{\left(N_0\right)_{fast}}\left(\frac{\mathrm{d}a_h(t)}{\mathrm{d}_t}\right)_{t\to 0,\,fast}} \tag{2}$$

where D_h is the effective diameter of particles, t is the time (min); N_0 is the density of

particles; K_{11} is the aggregation rate of RLA; $(K_{11})_{fast}$ is the aggregation rate of DLA.

The intersection of RLA regime and DLA regime is the CCC.

The aggregation rates were calculated by the average of the last 5 effective

diameters divided by the aggregation time at specific electrolyte concentration. The

fractal dimension in the DLA regime was obtained based on the method proposed by Wang et al. (2013).

$$D(t) = b * t^n + D_0 \qquad (3)$$

in which, $D(t)$ is the colloidal effective diameter at time t (min), D_0 is the initial effective diameter of colloids, and b and n are constants determined by the aggregation curves. The fractal dimension is $d_f = 1/n$ in the DLA regime.

3. Results and discussion

3.1 Particle size and distribution characteristics of Anthrosol and Calcisol colloidal fractions

The average diameters of Anthrosol and Calcisol colloids were measured by time-resolved DLS, and the results were shown in Table 1. The number-weighted diameters for Anthrosol colloids of $d < 2$ μm were about 1.04 times of $d < 1$ μm, and about 1.84 times of d < 100 nm, respectively. The intensity-weighted diameters for Anthrosol colloids were 294.10~396.81 nm. For Calcisol colloidal fractions, the number-weighted diameters for colloids of $d < 2$ μm were about 1.07 times of $d < 1$ μm, and about 1.65 times of d < 100 nm, and the intensity-weighted diameters were 312.25~439.20 nm. The intensity-weighted diameters were generally higher than the number-weighted diameters, especially in polydisperse system (Xu et al., 2020b). The colloidal particles in the soil solution were in constant Brownian motion, upon illumination by light, these colloidal particles scatter light, causing variations in light intensity. This phenomenon allowed for the calculation of the effective diameter of the particles, which was the intensity-weighted diameter (Filella et al., 1997). Given that particle diameter is

243   proportional to the sixth power of light intensity. Consequently, in polydisperse systems

244   where larger particles were present, the number-weighted diameter provided typically

245   a more accurate representation of the true diameter of colloidal particles (Xu et al.,

246   2015).

247   (*Insert Table 1 near here*)

248   From table 1, it can be seen that the average colloidal diameters of $d < 2$ μm were

249   close to that of $d < 1$ μm, and they were both significantly higher than that of the nano-

250   sized fraction. From the particle size distribution characteristics, it is clear that the size

251   range indicated by the differences of D_{90} and D_{10} increased with intended particle

252   diameter. For Anthrosol and Calcisol, 74.69% and 63.55% of all particles contained in

253   the colloidal suspensions of $d < 100$ nm were actually less than 100 nm, respectively,

254   indicating the complexity of soil colloidal particle irregularity.

255   **3.2 Physiochemical properties and clay mineralogy of Anthrosol and Calcisol**

256   **colloids**

257   Table 2 shows the physiochemical properties of soil colloidal fractions. The yields

258   of each colloidal fraction of Anthrosol were slightly larger than that of Calcisol,

259   respectively. The yields of colloidal particles of $d < 2$ μm were about 1.3~1.4 times of

260    $d < 1$ μm, and about 4.0~4.9 times of $d < 100$ nm, respectively. With the decreasing

261   colloidal particle diameter, the total carbon content, organic carbon and inorganic

262   carbon content all increased, suggesting the finer particles were richer in carbon. This

263   tendency is in agreement with other publications (Zhang et al., 2021; Said-Pullicino et

264   al., 2021; Hu et al., 2022). The specific surface areas for colloidal fractions of $d < 1$ μm

265 were largest of all, which may be related to the structures of formed clusters while

266 drying the samples for observation under microscopy (Yu et al., 2017; Weissenberger

267 et al., 2021). Furthermore, Anthrosol and Calcisol nanoparticles exhibited the lowest

268 specific surface area. This phenomenon raised from Organic substances adsorb

269 relatively little inorganic nitrogen (Li et al., 2013; Wilson et al., 2008). Therefore,

270 However, to our knowledge, no other better method has been reported for measuring

271 the specific surface area of natural nanoparticles.

272   (*Insert Table 2 near here*)

273   The clay mineralogy of Anthrosol and Calcisol colloidal fractions is shown in

274 Table 3. Calcisol colloidal fractions were dominant by illite, kaolinite and chlorite while

275 there was less chlorite in Anthrosol colloidal fractions. With the decrease of particle

276 size, the content of illite increased and kaolinite content decreased. This tendency is in

277 agreement with other publications (Chenu and Plante, 2006; Zhang et al., 2016). Among

278 the dominant clay types, the size of illite is finer than kaolinite and chlorite (Weil and

279 Brady, 2016), so its mass percentage was higher in the nano-sized fraction.

280   (*Insert Table 3 near here*)

281 **3.3 Surface properties of Anthrosol and Calcisol colloids**

282   The XPS spectra of soil colloidal fractions are shown in Fig. 1. From Fig. 1, it can

283 be seen that the main C-containing functional groups were C–C/C-H/C=C, C–O, C=O,

284 and COO- groups at 284.6, 286.2, 288.0 and 289.4 eV, respectively (Liang et al., 2020;

285 Ding et al., 2023). The functional groups for colloidal particles of $d < 100$ nm were

286 more abundant than those for colloids of $d < 2$ μm and $d < 1$ μm, while there were no

287   significant differences between colloids of $d < 2$ μm and $d < 1$ μm. With the decrease

288   of colloidal particle diameter, the relative contents of oxygen-containing functional

289   groups (C–O, C=O, COO-) gradually decreased. Specifically, the content decreased

290   gradually from 32.01% in Lou colloids of $d < 2$ μm to 20.93% in Lou colloids of $d <$

291   100 nm (Table S2). The functional groups of C–O and COO- gradually decreased until

292   they eventually disappeared, more C=O groups were exposed to the surrounding air.

293   For Calcisol colloids (Fig. 1d, e, f), the relative contents of organic oxygen-

294   containing functional groups for colloidal particles of $d < 2$ μm, $d < 1$ μm and $d < 100$

295   nm showed a different trend, compared with that in Anthrosol colloids. The relative

296   contents of organic oxygen-containing functional groups gradually increased with the

297   decrease of diameter. This trend was particularly pronounced in fraction of $d < 100$ nm,

298   and contents of C–O and COO- were highly increased (Table S2).

299   (*Insert Figure 1 near here*)

300   Oxygen-containing functional groups of C–O, C=O and COO- are electronegative

301   functional groups, hydroxyl and carboxyl groups can lose protons and make the surface

302   of soil colloidal particles carry negative charges (Audette et al., 2021). Functional

303   groups of C–O, C=O and COO- can affect the negative charges carried on the colloidal

304   surface by forming hydrogen bonds, and their polarity can also affect the negative

305   charges on the surface when O atom combines with C and H. The electrons will lean

306   towards the O atom with stronger electronegativity, which also makes the colloidal

307   surface carry negative charges (Tan et al., 2019). The contents and types of oxygen-

308   containing functional groups are one of the main factors affecting colloid charge and

309   aggregation.

310   The zeta potential values of different colloidal fractions at the pH range of 3–10

311   are shown in Fig. 2. Zeta potentials of the colloidal particles were negative, indicating

312   that they were negatively-charged. The zeta potentials of Anthrosol and Calcisol

313   colloidal particles were more negative with increasing solution pH, due to the

314   deprotonation of the surface (Moayedi and Kazemian, 2013; Dong et al., 2019).

315   Compared with the Calcisol colloids, the zeta potentials of Anthrosol colloidal particles

316   were more negative, due to Anthrosol possessed a higher surface charge density. For

317   Calcisol colloids, the differences among colloidal fractions were larger.

318   (*Insert Figure 2 near here*)

319   In general, zeta potential became more negative with increasing particle diameter.

320   When the pH changed from 3 to 10, for every pH unit increased, the zeta potential

321   values of Anthrosol colloids of $d < 2$ μm, < 1 μm, and < 100 nm would be increased by

322   2.14 mV, 2.09 mV and 1.89 mV; and for Calcisol colloids, those variation rates were

323   2.15 mV, 1.45 mV and 1.37 mV, respectively. Those data demonstrate that the charge

324   variability decreasing with the decreasing particle diameter. Song et al., (2019)

325   compared the zeta potential of wheat straw biochar nanoparticles (< 100 nm) and

326   colloidal particles (< 1000 nm), and found that the absolute values of colloidal particles

327   were larger at same pH, which was explained by the differences in the number of

328   surface carboxyl and hydroxyl groups. The zeta potential of colloidal particles is

329   proportional to charge density, which means that it is related to both charge quantity

330   and specific surface area (Hou et al., 2009). Therefore, the size effect of zeta potential

331   of Anthrosol and Calcisol colloidal particles is mainly related to the reduction of charge

332   density caused by larger specific surface area of nanoparticles (Xu et al. 2020b).

3.4 Aggregation kinetics curves of Anthrosol and Calcisol colloids in NaCl and CaCl$_2$ solutions

333

334

335   The aggregation kinetics of Anthrosol and Calcisol colloids in NaCl and CaCl$_2$

336   solutions are shown in Figs. S1 and S2. The aggregation process of soil colloids was

337   divided into RLA and DLA stages. The RLA stages for Anthrosol colloids of $d < 2$ μm,

338    $d < 1$ μm and $d < 100$ nm in NaCl solution were 0–80, 0–80 and 0–100 mmol·L^{-1},

339   respectively, during which repulsive forces existed between the particles and

340   attachment did not occur on every collision. As the electrolyte concentration continued

341   to increase, the solution entered into the DLA regime. At this point, attachment occurred

342   with every collision between particles, and the aggregation rates were not affected by

343   the electrolyte concentration. At last, the effective diameters of the formed clusters were

344   stable at around 1600 nm. Figure S1b, d and f showed that the aggregation behaviors

345   of Anthrosol colloids in CaCl$_2$ solution were similar to that in NaCl solution, and the

346   corresponding CaCl$_2$ concentrations for Anthrosol colloids of $d < 2$ μm, $d < 1$ μm and

347    $d < 100$ nm in RLA stage were about 0–1.5, 0–1.5 and 0–2 mmol·L^{-1}, respectively.

348   The aggregation kinetics of Calcisol colloids in NaCl and CaCl$_2$ solutions were

349   similar to Anthrosol colloids (Fig. S2). The RLA stages for Calcisol colloids of $d < 2$

350   μm, $d < 1$ μm and $d < 100$ nm in NaCl solution were 0–100, 0–120 and 0–250 mmol·L^{-1},

351   and were about 0–1.8, 0–1.7 and 0–2 mmol·L^{-1} in CaCl$_2$ solution, respectively. The

352   effective diameters of the clusters for Calcisol colloids were stabilized at about 1600

353   nm and 1800 nm in NaCl and CaCl$_2$ solutions, respectively.

354   Aggregation rates of soil colloids varied with particle diameters at the same

355 electrolyte concentration, which was particularly evident in RLA stage (Table 4). With

356 decreasing particle diameter, the aggregation rates of Anthrosol and Calcisol colloids

357 in 50 mmol·L^{-1} NaCl and 1 mmol·L^{-1} CaCl$_2$ solutions exhibited a corresponding

358 decline. In addition, in 50 mmol·L^{-1} NaCl solution, the aggregation rates for Anthrosol

359 colloids of $d < 2$ μm, $d < 1$ μm and $d < 100$ nm were about 2.17, 2.09 and 1.95 times

360 those of Calcisol colloids, while the aggregation rates were about 1.46, 1.57 and 1.91

361 times those of Calcisol colloids in 1 mmol·L^{-1} CaCl$_2$ solution, respectively. Therefore,

362 from table 4, the aggregation rates of Anthrosol and Calcisol colloids showed the size

363 effect. From table 4, it could be observed that the fractal dimensions in NaCl solutions

364 were largely higher than those in CaCl$_2$ solutions, suggesting a much denser structure

365 (Meng et al., 2013). In other words, the formed structures in divalent solutions were

366 more open.

367 (*Insert Table 4 near here*)

368 **3.5 Suspension stability of Anthrosol and Calcisol colloids in NaCl and CaCl$_2$**

369 **solutions**

370 The CCCs for Anthrosol colloids of $d < 2$ μm, $d < 1$ μm and $d < 100$ nm in NaCl

371 solution were 80.40, 91.78 and 134.96 mmol·L^{-1}, respectively (Fig. 3a), and those for

372 Calcisol colloids were 121.10, 126.50 and 292.86 mmol·L^{-1}, respectively (Fig. 3b). The

373 CCCs increased with the decreasing particle diameter, indicating that the suspension

374 stability of soil nanoparticles was stronger than those of colloidal particles.

375 (*Insert Figure 3 near here*)

376 In CaCl$_2$ solutions, the CCCs for Anthrosol colloids of $d < 2$ μm, $d < 1$ μm and d

18

377 < 100 nm were 1.61, 1.68 and 1.77 mmol·L^{-1}, respectively, and for Calcisol colloids,

378 those corresponding values were 1.90, 1.91 and 2.13 mmol·L^{-1} (Fig. 4). The CCCs in

379 CaCl$_2$ solutions also increased with the decreasing particle size. The contents of K$^+$,

380 Na$^+$, Ca^{2+} and Mg^{2+} in Anthrosol and Calcisol colloidal suspensions decreased with the

381 decreasing colloidal particle diameter (Table S3), which was mainly due to the dilution

382 effect during the extraction process. Furthermore, Table S3 showed that the soluble

383 cation contents were rather low, and their effects on the CCCs of soil colloids could be

384 neglected.

385   (*Insert Figure 4 near here*)

386   Based on Figs. 3 and 4, 3 mmol·L^{-1} CaCl$_2$ solution could cause fast aggregation

387 of soil colloidal particles, while it required at least 80 mmol·L^{-1} NaCl solution for

388 comparable aggregation rate, indicating that the shielding effect of divalent cations on

389 negative charges of colloids was stronger than that of monovalent cations. The

390 quantitative calculation results showed that the CCC ratios of monovalent ion and

391 divalent ion system were between 25.64 and 27.09, which conformed to the Schulze-

392 Hardy rule (Baalousha, 2017).

393   For each type of the soil colloids, the higher the absolute zeta potential values of

394 colloidal particles, the more negative charges carried on the surface, and the higher the

395 stability (CCCs) of suspension. For the same particle diameter, e.g. d < 100 nm, the

396 absolute zeta potentials of Anthrosol colloids were larger (Fig. 2) while the

397 corresponding CCC was lower (Figs. 3 and 4). Study on the stability of biochar

398 nanoparticles showed that the absolute values of zeta potentials could not be used to

399 directly explain the stability difference among biochar nanoparticles from different

400 feedstock materials but could explain the influences of solution conditions on the

401 stability of biochar nanoparticles derived from the same feedstock material (Xu et al.,

402 2020a).

403 The CCCs of Anthrosol and Calcisol colloids increased with decreasing diameter;

404 that is, the CCCs of Anthrosol and Calcisol colloids both showed the size effects. Hsu

405 and Kuo (1995) demonstrated that the CCCs would generally decrease with the

406 increasing particle diameter because smaller particles possess thicker double electric

407 layers and higher electrolyte concentration is needed to neutralize charges on the

408 surface, which were consistent with the results of Anthrosol and Calcisol colloids. The

409 above explanation by Hsu and Kuo (1995) was derived from homogenous particles

410 whose composition does not change with particle diameter. The results of this paper

411 show that, for those two alkaline soils being such heterogeneous materials, when the

412 organic matter contents and mineral types changed with colloidal particle diameter, the

413 CCCs in monovalent and divalent solutions also decreased with increasing particle

414 diameter.

415 In this paper, the organic matter contents of soil nanoparticles were the highest, so

416 the CCCs were the largest, which were 1.7 and 2.4 times of the corresponding colloidal

417 particles of $d < 2$ μm. The suspension stability of different clay minerals has been

418 reported to vary with the mineralogical structure. The CCC of illite (≈ 100 mM) in

419 NaCl solution was significantly higher than that of kaolinite (≈ 20 mM) (Jiang et al.,

420 2012; Xu et al., 2017), indicating that the stability of illite suspensions is significantly

higher than that of kaolinite. So another possible reason for the higher stability of soil nanoparticles is the increase of illite content and the decrease of kaolinite content. Therefore, the differences in organic matter contents and clay mineralogy are the fundamental reasons for the differences in colloidal suspension stability behind the size effects of Anthrosol and Calcisol colloids.

4. Conclusion

This study obtained soil colloidal fractions with three different particle sizes from Anthrosol and Calcisol using high-speed centrifugation and revealed the particle size effects on the soil constitutes, surface properties, and aggregation behavior of heterogeneous soil colloids. The results showed that, compared to coarse colloids ($d <$ 2 μm and $d <$ 1 μm), the organic carbon contents of Anthrosol and Calcisol nanoparticles were higher, at 27.38 $g·kg^{-1}$ and 28.31 $g·kg^{-1}$, respectively, approximately twice and three times that of the coarse colloids and the bulk soils, indicating that nanoparticles exhibit a strong potential for carbon sequestration. The absolute zeta potential values of soil nanoparticles decreased with decreasing average particle diameter, indicating a reduction in charge density. Anthrosol and Calcisol nanoparticles exhibited greater suspension stability in NaCl and $CaCl_2$ solutions. On one hand, this was due to the increased thickness of the double electric layer on the surface of soil nanoparticles, resulting in stronger repulsive forces between particles; on the other hand, it was due to the presence of more illite, which has higher CCC compared to other clay minerals. In conclusion, for such a highly heterogeneous system as soil, the size effects on soil colloidal suspension stability are strongly influenced by

variations driven by essentially mineral composition. Future studies should further explore the mechanisms underlying the size effects of the typical soils on particle interactions, coagulation, and transport behaviors under environmentally relevant conditions.

Acknowledgments

Author Contributions

Conceptualization, Xu, C.Y., Geng, Z.C., and Hu, F.N.; methodology, Xu, C.Y.; software, Yan, Y.Y.; formal analysis, Liu, J.J.; investigation, Zhang, X.R.; resources, Yan, Y.Y.; writing—original draft, Yan, Y.Y.; writing—review and editing, Xu, C.Y., and Hu, F.N.; visualization, Xu, C.Y., and Yan, Y.Y.; funding acquisition, Xu, C.Y., Geng, Z.C. and Hu, F.N.. All authors have read and agreed to the published version of the manuscript.

Declaration of Interest Statement

The authors declare that they have no known competing financial interests or personal relationships that could have appeared to influence the work reported in this paper.

463

References

Audette, Y., Congreves, K.A., Schneider, K., Zaro, G.C., Nunes, A.L.P., Nunes, A.L.P., Zhang, H.J., Voroney, R.P.: The effect of agroecosystem management on the distribution of C functional groups in soil organic matter: A review. Biol. Fertil. Soils. 57, 881–894, 2021.

Baalousha, M.: Aggregation and disaggregation of iron oxide nanoparticles: Influence of particle concentration, pH and natural organic matter. Sci. Total Environ. 407(6), 2093–2101, 2009.

Baalousha, M.: Effect of nanomaterial and media physicochemical properties on nanomaterial aggregation kinetics. NanoImpact. 6, 55–68, 2017.

Cárdenas, J.P., Santiago, A., Tarquis, A.M., Losada, J.C., Borondo, F., Benito, R.M.: Soil porous system as heterogeneous complex network. Geoderma. 160(1), 13–21, 2010.

Chen, K.L., Elimelech, M.: Aggregation and deposition kinetics of Fullerene (C_{60}) nanoparticles. Langmuir 22, 10994–11001, 2006.

Chenu, C., Plante, A.F.: Clay-sized organo-mineral complexes in a cultivation chronosequence: revisiting the concept of the'primary organo-mineral complex'. Eur J Soil Sci. 57(4), 596–607, 2006.

Ding, W., Liang, H.X., Zhang, H.W., Sun, H., Geng, Z.C., Xu, C.Y.: A cellulose/bentonite grafted polyacrylic acid hydrogel for highly-efficient removal of Cd(II). J. Water Process. Eng. 51, 103414, 2023.

Dong, S.N., Zeng, Z., Cai, W.W., Zhou, Z.Y., Dou, C.B., Liu, H., Xia, J.H.: The zeta potentials of g-C$_3$N$_4$ nanoparticles: Effect of electrolyte, ionic strength, pH, and humic acid. J. Nanopart Res. 21, 233, 2019.

Filella, M., Zhang, J.W., Newman, M.E., Buffle, J.: Analytical applications of photon correlation spectroscopy for size distribution measurements of natural colloidal suspensions: capabilities and limitations. Colloid Surf. A. 120(1–3), 27–46, 1997.

He, Y.T., Wan, J., Tokunaga, T.: Kinetic stability of hematite nanoparticles, The effect of particle sizes. J. Nanopart Res. 10, 321–332, 2008.

Hou, J., Li, H., Zhu, H.L.,Wu, L.S.: Determination of clay surface potential, a more reliable approach. Soil Sci Soc Am J. 73(5), 1658–1663, 2009.

Hsu, J.P., Kuo, Y.C.: An Extension of the Schulze-Hardy Rule to Asymmetric Electrolytes. J. Colloid Interface Sci. 171(1), 254–255, 1995.

Hu, N., Xu, C.Y., Geng, Z.C., Hu, F.N., Li, Q.R., Ma, R.T., Wang, Q.: The interplay of particle properties and solution chemistry on aggregation kinetics of soil nanoparticles. J Soils Sediments. 22, 1761–1772, 2022.

IUSS Working Group WRB. World Reference Base for Soil Resources. International soil classification system for naming soils and creating legends for soil maps. 4th edition. International Union of Soil Sciences (IUSS), Vienna, Austria. 2022.

Jiang, C.L., Séquaris, J.M., Vereecken, H., Klumpp, E.: Effects of inorganic and organic anions on the stability of illite and quartz soil colloids in Na-, Ca- and mixed Na-Ca systems. Colloids Surf. A. 415, 134–141, 2012.

Lead, J.R., Wilkinson, K.J.: Aquatic Colloids and Nanoparticles: Current Knowledge

and Future Trends. Environ. Chem. 3(3), 159–171, 2006.

Li, S.X., Luo, Y.M., Zhang, H.B., Huang, Y.J., Li, Z., Wei, J.: Arsenic forms in various particle-size fractions of red soil-Chemical fractionation and speciation using XANES analysis. Acta Scientiae Circumstantiae. 31(12), 2733–2739, 2011.

Li, W. Y., Zhu, X.Y., He, Y., Xing, B. S., Xu, J.M.: Enhancement of water solubility and mobility of phenanthrene by natural soil nanoparticles. Environ Pollut. 176, 228–233, 2013.

Liang, H.X., Sun, R.R., Song, B., Sun, Q.Q., Peng, P., She, D.: Preparation of nitrogen-doped porous carbon material by a hydrothermal-activation two-step method and its high-efficiency adsorption of Cr(VI). J. Hazard. Mater. 387, 121987, 2020.

Liu, G., Zheng, H., Jiang, Z., Zhao, J., Wang, Z., Pan, B., Xing, B.: Formation and physicochemical characteristics of nano biochar: insight into chemical and colloidal stability. Environ. Sci. Technol. 52(18), 10369–10379, 2018.

Luo, J.J., Niu, Q., Jin, M.C., Cao, Y.A., Ye, L.R., Du, R.P.: Study on the effects of oxygen-containing functional groups on Hg^0 adsorption in simulated flue gas by XAFS and XPS analysis. J. Hazard. Mater. 376(15), 21–28, 2019.

Mashayekhi, H., Ghosh, S., Du, P., Xing, B.: Effect of natural organic matter on aggregation behavior of C60 fullerene in water. J. Colloid Interf. Sci. 374(1), 111–117, 2012.

Mayordomo, N., Degueldre, C., Alonso, U., Missana, T.: Size distribution of FEBEX bentonite colloids upon fast disaggregation in low-ionic strength water. Clay Miner. 51(2), 213–222, 2016.

529   Meng, Z.Y., Hashmi, S.M., Elimelech, M.: Aggregation rate and fractal dimension of

530   fullerene nanoparticles via simultaneous multiangle static and dynamic light

531   scattering measurement. J. Colloid Interface Sci. 392, 27–33, 2013.

532   Moayedi, H., Kazemian, S.: Zeta potentials of suspended humus in multivalent cationic

533   saline solution and its effect on electro-osomosis behavior. J. Dispers Sci. Technol.

534   34(2), 283–294, 2013.

535   Said-Pullicino, D., Giannetta, B., Demeglio, B., Missong, A., Gottselig, N., Romani,

536   M., Bol, R., Klumpp, E., Celi, L.: Redox-driven changes in water-dispersible

537   colloids and their role in carbon cycling in hydromorphic soils. Geoderma. 385,

538   114894, 2021.

539   Schäfer, T., Huber, F., Seher, H., Missana, T., Alonso, U., Kumke, M., Eidner, S., Claret,

540   F., Enzmann, F.: Nanoparticles and their influence on radionuclide mobility in

541   deep geological formations. Appl. Geochemistry. 27(2), 390–403, 2012.

542   Song, B.Q., Chen, M., Zhao, L., Qiu, H., Cao, X.D.: Physicochemical property and

543   colloidal stability of micron- and nano-particle biochar derived from a variety of

544   feedstock sources. Sci. Total Environ. 661, 685–695, 2019.

545   Sun, Y.L., Pan, D.Q., Wei, X.Y., Xian, D.F., Wang, P., Hou, J.J.: Insight into the stability

546   and correlated transport of kaolinite colloid: Effect of pH, electrolytes and humic

547   substances. Environ. Pollut. 266, 115189, 2020.

548   Tan, Z.X., Yuan, S.N., Hong, M.F., Zhang, L.M., Huang, Q.Y.: Mechanism of negative

549   surface charge formation on biochar and its effect on the fixation of soil Cd. J.

550   Hazard. Mater. 384, 121370, 2019.

551 Tang, Y., Li, H., Liu, X.M., Zhu, H.L., Tian, R.: Unraveling the size distributions of

552   surface properties for purple soil and yellow soil. J Environ Sci (China). 32, 81–

553   89, 2015.

554 Tsao, T.M., Chen, Y.M., Sheu, H., Tzou, Y.M., Chou, Y.M., Wang, M.K.: Separation

555   and identification of soil nanoparticles by conventional and synchrotron X-ray

556   diffraction. Appl. Clay Sci. 85, 1–7, 2013.

557 Tsao, T.M., Chen, Y.M., Wang, M.K., Huang, P.M.: Structural transformation and

558   physicochemical properties of environmental nanoparticles by comparison of

559   various particle-size fractions. Soil Sci Soc Am J. 75(2), 533–541, 2011.

560 Wang, L.F., Wang, L.L., Ye, X.D., Li, W.W., Ren, X.M., Sheng, G.P., et al.: Coagulation

561   kinetics of humic aggregates in mono-and divalent electrolyte solutions. Environ.

562   Sci. Technol. 47(10), 5042–5049, 2013.

563 Wang, Q.R., Li, Y.C., Wang, Y.: Optimizing the weight loss-on-ignition methodology

564   to quantify organic and carbonate carbon of sediments from diverse sources.

565   Environ. Monit. Assess. 174, 241–257, 2011.

566 Wei, X.Y., Pan, D.Q., Xu, Z., Xian, D.F., Li, X.L., Tan, Z.Y., Liu, C.L., Wu, W.S.:

567   Colloidal stability and correlated migration of illite in the aquatic environment:

568   The roles of pH, temperature, multiple cations and humic acid. Sci. Total Environ.

569   768, 144174, 2021.

570 Weil, R.R., Brady, N.C.: The Nature and Properties of Soils, Global Edition. Pearson

571   Education Limited. 2016.

572 Weissenberger, G., Henderikx, R.J., Peters, P.J.: Understanding the invisible hands of

573 sample preparation for cryo-EM. Nat. Methods. 18(5), 463–471, 2021.

574 Wilson, M. A., Tran, N. H., Milev, A. S., Kannangara, G. S. K., Volk, H.: Nanomaterials

575   in soils. Geoderma. 146, 291–302, 2008.

576 Won, J., Burns, S.E.: Role of Immobile Kaolinite Colloids in the Transport of Heavy

577   Metals. Environ. Sci. Technol. 52(5): 2735–2741, 2018.

578 Xu, C.Y., Deng, K.Y., Li, J.Y., Xu, R.K.: Impact of environmental conditions on

579   aggregation kinetics of hematite and goethite nanoparticles. J. Nanopart Res. 17,

580   394, 2015.

581 Xu, C.Y., Li, Q.R., Geng, Z.C., Hu, F.N., Zhao, S.W.: Surface properties and suspension

582   stability of low–temperature pyrolyzed biochar nanoparticles: Effects of solution

583   chemistry and feedstock sources. Chemosphere. 259, 127510, 2020a.

584 Xu, C.Y., Xu, R.K., Li, J.Y., Deng, K.Y.: Phosphate-induced aggregation kinetics of

585   hematite and goethite nanoparticles. J. Soils Sediments. 17, 352–363, 2017.

586 Xu, C.Y., Zhou, T.T., Wang, C.L., Liu, H.Y., Zhang, C.T., Hu, F.N., Zhao, S.W., Geng,

587   Z.C.: Aggregation of polydisperse soil colloidal particles: Dependence of

588   Hamaker constant on particle size. Geoderma. 359, 113999, 2020b.

589 Xu, Z., Pan, D.Q., Sun, Y.L., Wu, W.S.: Stability of GMZ bentonite colloids:

590   Aggregation kinetic and reversibility study. Appl. Clay Sci. 161, 436–443. 2018.

591 Yin, X.Q., Gao, B., Ma, L.Q., Saha, U.K., Sun, H.M., Wang, G.D.: Colloid-facilitated

592   Pb transport in two shooting-range soils in Florida. J. Hazard. Mater. 177(1–3),

593   620–625, 2010.

594 Yu, X., Fu, Y., Lu, S.: Characterization of the pore structure and cementing substances

of soil aggregates by a combination of synchrotron radiation X-ray micro–

computed tomography and scanning electron microscopy. Eur. J. Soil Sci. 68(1),

66–79, 2017.

Zhang, Q., Bol, R., Amelung, W., Missong, A., Siemens, J., Mülder, I.: Water

dispersible colloids and related nutrient availability in Amazonian Terra Preta soils.

Geoderma. 397, 115103, 2021.

Zhang, Z.Y., Huang, L., Liu, F., Wang, M.K., Fu, Q.L., Zhu, J.: Characteristics of clay

minerals in soil particles of two Alfisols in China. Appl. Clay Sci. 120, 51–60,

2016.

Zhou, D.X., Ji, Z.X., Jiang, X.M., Dunphy, D.R., Brinker, J., Keller A.A.: Influence of

material properties on TiO_2 nanoparticle agglomeration. PLoS One. 8(11), e81239,

2013.

Zhu, X., Chen, H., Li, W., He, Y., Brookes, P.C., Xu, J.: Aggregation kinetics of natural

soil nanoparticles in different electrolytes. Eur. J. Soil Sci. 65(2), 206–217, 2014.

611 **Table captions**

612 **Table 1** The average diameters and distribution patterns of soil colloids.

613 **Table 2** The physiochemical properties of soil colloids.

614 **Table 3** The dominant clay minerals of soil colloidal fractions (shown in mass

615 fraction, %).

616 **Table 4** The aggregation rates of soil colloids.

617

618 **Table 1** The average diameters and distribution patterns of soil colloids

Soil type	Colloidal fractions	Number-weighted diameter (nm)	Intensity-weighted diameter (nm)	D_{10} (nm)	D_{90} (nm)
Anthrosol	$d < 2$ μm	133.16 ± 24.28	396.81 ± 12.34	71.53	232.49
	$d < 1$ μm	127.84 ± 20.29	371.45 ± 11.88	67.64	219.87
	$d < 100$ nm	72.47 ± 7.04	294.10 ± 15.80	38.74	136.72
Calcisol	$d < 2$ μm	141.23 ± 24.33	439.20 ± 12.72	78.29	244.97
	$d < 1$ μm	131.67 ± 15.77	372.07 ± 8.23	75.84	231.64
	$d < 100$ nm	85.48 ± 16.93	312.25 ± 33.58	47.84	158.99

619 Note: D_{10}, D_{50} and D_{90} represent diameter of particles with a cumulative distribution of 10%, 50% and
620 90%, respectively.

621

Table 2 The physiochemical properties of soil colloids

Soil type	Colloidal fractions	Yield (%)	Total carbon content ($g \cdot kg^{-1}$)	Organic carbon content ($g \cdot kg^{-1}$)	CaCO$_3$ content ($g \cdot kg^{-1}$)	Specific surface area ($m^2 \cdot g^{-1}$)
Anthrosol	$d < 2$ μm	25.12	20.90 ± 0.30	10.90 ± 1.29	10.00	65.37
	$d < 1$ μm	18.76	20.65 ± 0.15	10.91 ± 0.43	9.74	72.99
	$d < 100$ nm	6.32	58.25 ± 0.35	27.38 ± 0.21	30.87	45.28
Calcisol	$d < 2$ μm	23.17	24.00 ± 0.30	11.66 ± 0.60	12.34	49.99
	$d < 1$ μm	16.20	22.30 ± 0.20	12.76 ± 0.11	9.54	61.88
	$d < 100$ nm	4.70	76.30 ± 0.40	28.31 ± 0.15	47.99	34.53

623

624   **Table 3** The dominant clay minerals of soil colloidal fractions (shown in mass fraction, %)

Soil type	Colloidal fractions	Illite	Kaolinite	Chlorite	Vermiculite
Anthrosol	$d < 2$ μm	34	23	4	9
	$d < 1$ μm	30	22	7	11
	$d < 100$ nm	37	14	16	3
Calcisol	$d < 2$ μm	24	22	29	16
	$d < 1$ μm	31	19	25	12
	$d < 100$ nm	37	16	17	5

625

Table 4 The aggregation rates of soil colloids

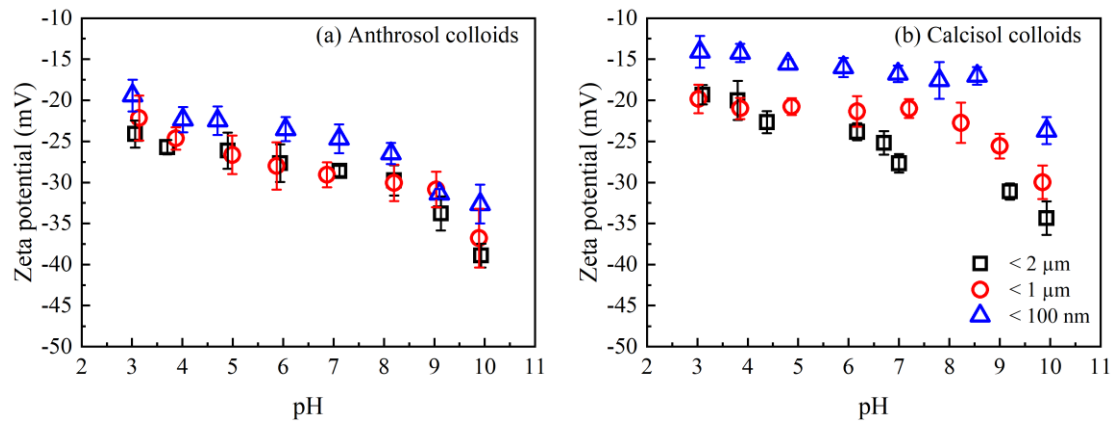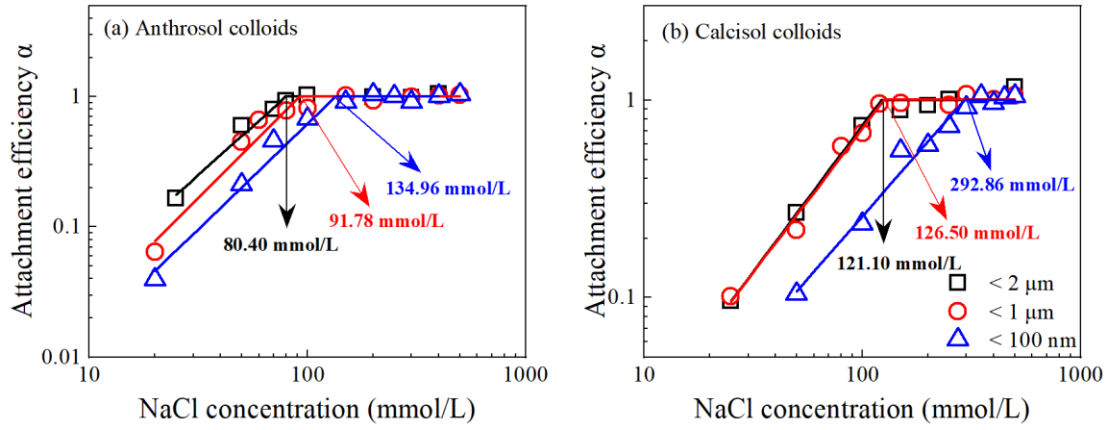| Soil type	Colloidal fractions	Aggregation rate		Fractal dimension	
		In 50 mmol·L^{-1} NaCl (nm·min^{-1})	In 1 mmol·L^{-1} CaCl$_2$ (nm·min^{-1})	Na	Ca
Anthrosol	$d < 2$ μm	19.46	12.01	1.69 ± 0.19	1.33 ± 0.26
	$d < 1$ μm	14.91	11.48	1.75 ± 0.06	1.52 ± 0.19
	$d < 100$ nm	7.72	9.97	1.71 ± 0.26	1.68 ± 0.13
Calcisol	$d < 2$ μm	8.98	8.22	1.30 ± 0.17	1.36 ± 0.17
	$d < 1$ μm	7.15	7.33	1.71 ± 0.24	1.30 ± 0.31
	$d < 100$ nm	3.95	5.22	1.52 ± 0.22	1.58 ± 0.19

627

628 **Figure captions**

629 **Fig. 1.** The photoelectron spectrum C1s and O1s peak diagram of Anthrosol and

630 Calcisol colloids. C1s of Anthrosol colloids, a. $d < 2$ μm, b. $d < 1$ μm, c. $d < 100$ nm;

631 C1s of Calcisol colloids, d. $d < 2$ μm, e. $d < 1$ μm, f. $d < 100$ nm; O1s of Anthrosol

632 colloids, g. $d < 2$ μm, h. $d < 1$ μm, i. $d < 100$ nm; O1s of Calcisol colloids, j. $d < 2$ μm,

633 k. $d < 1$ μm, l. $d < 100$ nm.

634 **Fig. 2.** The zeta potential of Anthrosol (a) and Calcisol (b) colloids of $d < 2$ μm, < 1 μm,

635 and < 100 nm at different pH

636 **Fig. 3.** The CCCs of Anthrosol (a) and Calcisol (b) colloids of $d < 2$ μm, < 1 μm, and $<$

637 100 nm in NaCl solution

638 **Fig. 4.** The CCC of Anthrosol (a) and Calcisol (b) colloids of $d < 2$ μm, < 1 μm, and $<$

639 100 nm in CaCl2 solution
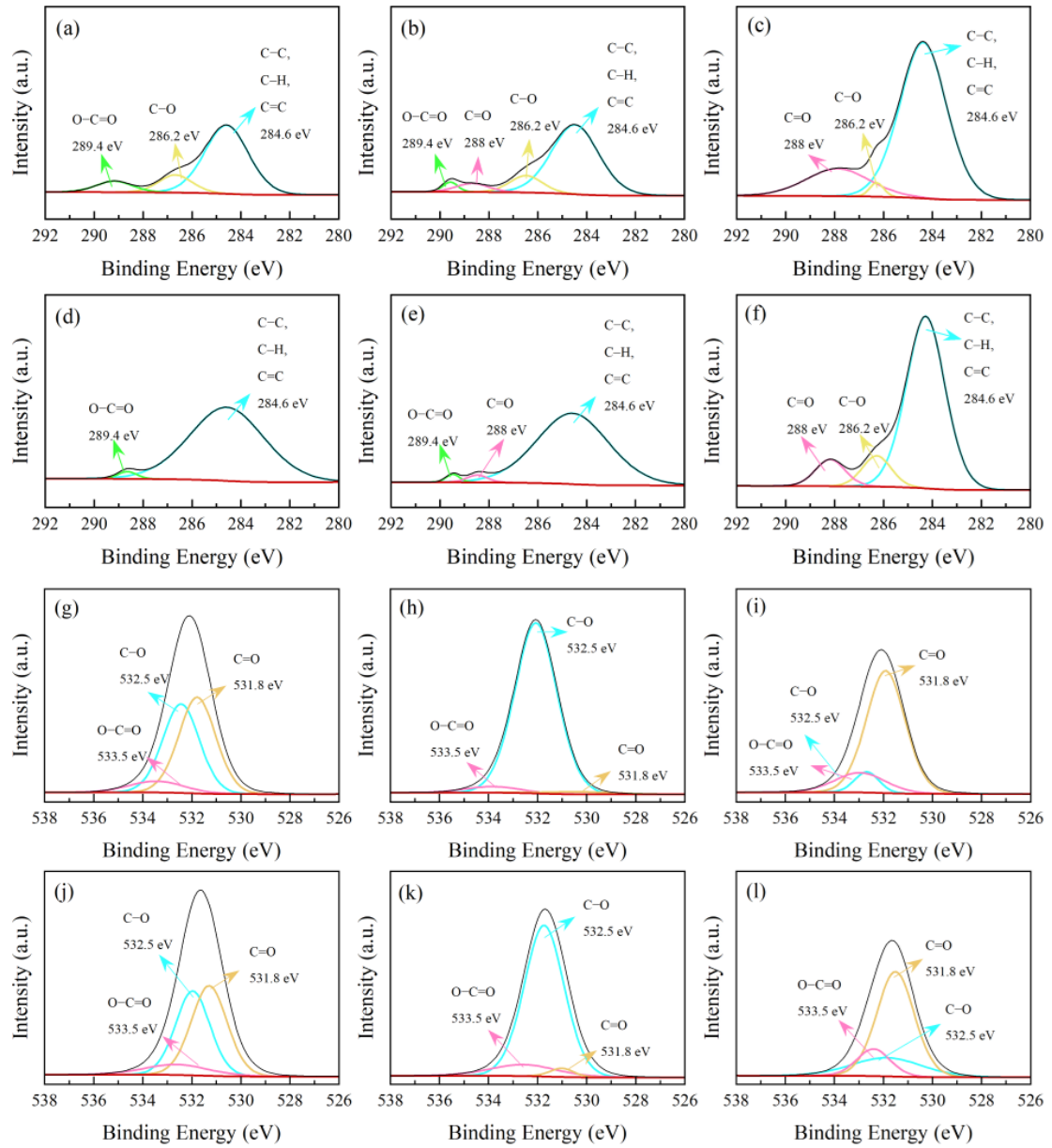
Fig. 1 The photoelectron spectrum C1s and O1s peak diagram of Anthrosol and Calcisol colloids. C1s of Anthrosol colloids, (a). $d < 2$ μm, (b). $d < 1$ μm, (c). $d < 100$ nm; C1s of Calcisol colloids, (d). $d < 2$ μm, (e). $d < 1$ μm, (f). $d < 100$ nm; O1s of Anthrosol colloids, (g). $d < 2$ μm, (h). $d < 1$ μm, (i). $d < 100$ nm; O1s of Calcisol colloids, (j). $d < 2$ μm, (k). $d < 1$ μm, (l). $d < 100$ nm.

647

Fig. 2 The zeta potential of Anthrosol (a) and Calcisol (b) colloids of $d < 2$ μm, < 1 μm, and $<$ 100 nm at different pH
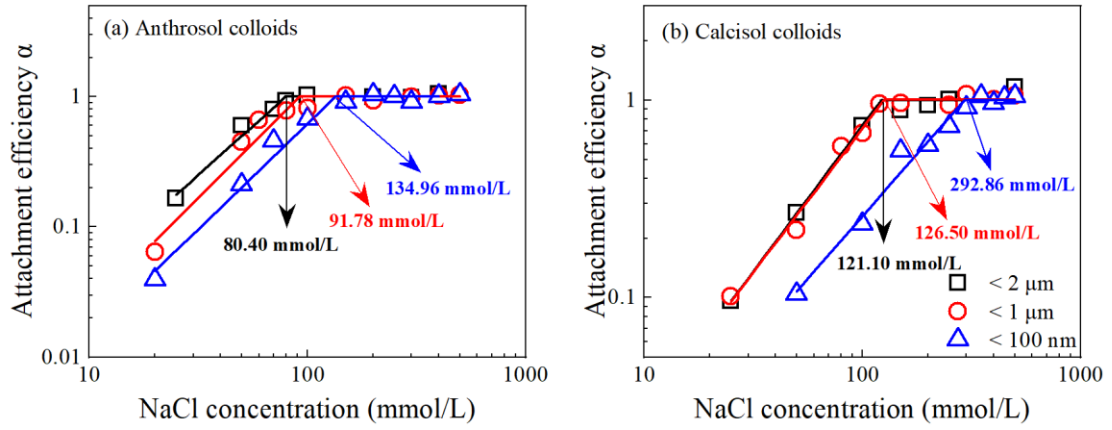
650

Fig. 3 The CCCs of Anthrosol (a) and Calcisol (b) colloids of d < 2 μm, < 1 μm, and < 100 nm in NaCl solution

Fig. 4 The CCC of Anthrosol (a) and Calcisol (b) colloids of $d <$ 2 μm, < 1 μm, and < 100 nm in CaCl$_2$ solution。